JOURNAL OF MATERIALS SCIENCE 10 (1975) 1465–1471

Application of fracture mechanics to plastics deformed at high strain-rates

Part 2 *Geometrical factors*

H. V. SQUIRES, P. E. REED
Department of Materials, Queen Mary College, University of London, UK

The effects of wall thickness and tube length on the fracture strength of thin walled cylindrical specimens of poly(methylmethacrylate) containing artificial flaws is examined. Data obtained are compared with that predicted by fracture mechanics theory developed for quasi-static conditions. Special attention is given to corrections for finite width and bending effects under dynamic loading conditions. It is concluded that the fracture mechanics relationships derived for quasi-static conditions, with the exception of the bending correction factor, are applicable to the dynamic situation with reasonable accuracy. It is further concluded that, for accurate analysis, the effect of dynamic loading on the stress field, and possibly the stress intensity factor, must be taken into consideration.

1. Introduction

Fracture mechanics is now applied to a variety of engineering problems to relate the applied stress to the maximum permissible flaw size. The relationship varies with the geometry of the item containing the flaw [1, 2], but generally takes the form

$$\sigma = Aa^{-\frac{1}{2}} \tag{1}$$

where σ is the applied stress, a is the semi-crack length and A is a constant for a particular specimen geometry and testing condition. For a flat plate of infinite width containing a centre notch of length $2a$, Equation 1 can take the form

$$\sigma_f = K_{IC}(\pi a)^{-\frac{1}{2}} \tag{2}$$

where K_{IC} is the critical stress intensity factor and σ_f the fracture stress. Alternatively, the fracture criterion has been expressed by Griffith [3] as

$$\sigma_f = \left(\frac{2E\gamma}{\pi a}\right)^{\frac{1}{2}} \tag{3}$$

where E is the elastic modulus for the material and γ the specific surface energy. Comparing Equations 2 and 3, it is seen that $K_{IC} = (2E\gamma)^{\frac{1}{2}}$ for the particular case considered. Since both E and γ are material parameters, it at first appeared that K_{IC} might be a universal constant. However, attempts to fit Equations 2 and 3 to experimental data for most materials, especially plastics, showed that K_{IC} was both strain-rate [4] and specimen geometry dependent [1, 2], and that γ was considerably larger than theoretically possible [5]. The fact that the "constants" in the equations are not universal emphasizes the need to test different specimen configurations under different conditions.

A previous paper [6] commented on the fracture of thin walled cylindrical specimens of poly(methylmethacrylate) (PMMA) when subjected to internal shock pressure pulses. It was found that a function of the form

$$\sigma_\theta = \left(\frac{2E\gamma}{\pi a}\right)^{\frac{1}{2}} - \sigma_\infty \tag{4}$$

fitted the experimental data for the hoop stress, σ_θ, for fracture, and that the values of E and γ differed only slightly from those required to fit quasi-static data for the same material. Equation 4 differs from the previous equations by the inclusion of the constant σ_∞. Practical considerations dictate that $\sigma_\theta \to 0$ as $a \to \infty$ and hence attempts were made to eliminate σ_∞ by applying finite width and bending correction factors, but without complete success. The previous work on shock loading of flawed PMMA tubes has now been extended to study the effects of varying the tube length and wall thickness on the fracture

behaviour. Williams and Ewing have reported on the application of fracture mechanics to cylindrical tubes subjected to quasi-static internal pressure [2]. They found that a relationship of the form

$$\sigma_\theta = K(\pi a)^{-\frac{1}{2}} \left(1 + 1.67 \frac{a^2}{Rt}\right)^{-\frac{1}{2}} \quad (5)$$

fitted their data, where $[1 + 1.67(a^2/Rt)]^{-\frac{1}{2}}$ was the bending correction factor theoretically derived by Folias [7].

2. Experimental

Details of the technique used for impact testing the tubular specimens have been described previously [6, 8]. A shock tube is used to apply a step impulse to the specimen, which forms an integral part of the shock tube. The specimen is mounted so that it is essentially a freely supported body. Under the action of the internal pressure pulse, the tube can expand radially along its entire length with minimal end restraint. The artificial crack of length $2a$ is inserted in the specimen as shown in Fig. 1, by drilling a hole at one end of the intended crack and traversing the drill along a generator of the tube. The ends of the crack are then sharpened with a razor. The possible geometrical variables of the specimen are the length (W), crack length ($2a$) and the wall thickness (t). The internal radius (R) of the specimen is dictated by the size of the shock tube, since the bores of the specimen and shock tube must be identical to form a smooth continuation of each other.

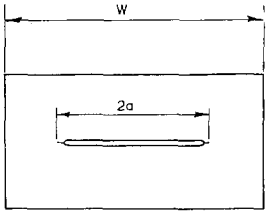

Figure 1 Schematic of specimen geometry depicting the location of the artificially inserted flaw in the tube wall.

Sets of PMMA specimens were machined, each set containing approximately fifteen specimens. The wall thickness and specimen length were held constant throughout each set while the crack lengths were varied to give crack length to specimen width ratios in the range $0.015 \leq 2a/W \leq 0.75$. Four sets were tested; three with the specimen length constant at 50.8 mm but different thicknesses of 0.38, 0.762 and 1.525 mm respectively, and the fourth of length 25.4 mm and wall thickness 0.762 mm. The lower value of wall thickness used was dictated by machining limitations, while the upper limit was determined by the magnitude of the pressure pulses that could be obtained with the shock tube used which would fracture the thick walled tubes containing short cracks. The shock tube was operated in primary shock loading mode [8], i.e. the shock pulse travelling through the specimen once to exhaust. Each specimen was subjected to a sequence of shock pulses of increasing magnitude until fracture occurred.

Since the ends of the specimen are open and unrestrained, the stress system acting in the flawed cylinders is considered to be predominantly a unidirectional circumferential stress, σ_θ. For a thin walled cylinder of mean radius (R), wall thickness (t) subjected to an internal pressure (p), the circumferential stress is given by

$$\sigma_\theta = p \frac{R}{t} \cdot \quad (6)$$

This equation is derived from equilibrium considerations and is strictly applicable only to membranes. It has been shown previously [6] that, when fracture propagates from the artificial crack, it initiates at the inside edge of that crack. The circumferential stress at the bore of a tube of finite thickness under internal pressure, again for equilibrium conditions, is given by the "thick wall cylinder" equation [9],

$$\sigma_\theta = p \frac{(R_o^2 + R_i^2)}{(R_o^2 - R_i^2)} \quad (7)$$

where R_o and R_i are the external and internal radii of the specimen respectively. Values of σ_θ derived by Equation 7 were found to be $\frac{1}{2}$, 1 and 2% greater than those derived from Equation 6 for the 0.38, 0.762 and 1.525 mm thick specimens, respectively. In the present paper, the small correction for finite tube thickness has been applied and hoop stresses quoted have been derived from Equation 7 before other correction factors are applied.

3. Application of correction factors to impact data

3.1. Fracture stress versus crack length

Fig. 2 shows the variation of the hoop stress at fracture with crack length for all four sets of

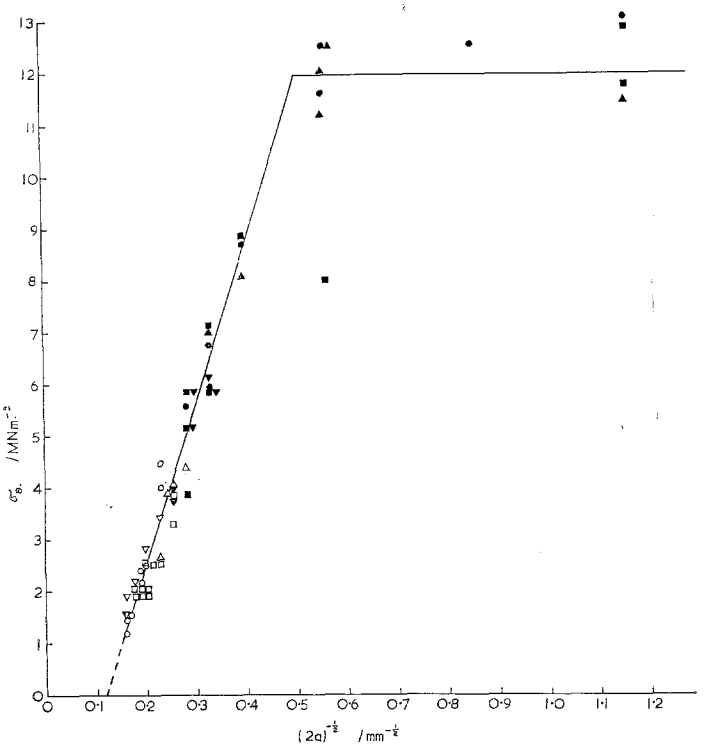

Figure 2 Variation of fracture stress with $(2a)^{-\frac{1}{2}}$ for all specimens tested (σ_θ is the maximum hoop stress derived from thick cylinder formulae). ■/□ Tube length 50.8 mm, wall thickness 0.38 mm; ●/○ tube length 50.8 mm, wall thickness 0.76 mm; ▼/▽ tube length 50.8 mm, wall thickness 1.52 mm; ▲/△ tube length 25.4 mm, wall thickness 0.76 mm. Filled symbols indicate fragmentation; open symbols indicate single crack propagation.

specimens. The open symbols indicate fracture by the propagation of a single crack from the ends of the initial inserted crack. In such cases, the path of the fracture plane continued the inserted crack along a generator of the tube, and was therefore normal to the direction of the applied stress. This mode of fracture will be referred to as the single fracture mode. Filled symbols indicate that the specimen shattered at fracture into a large number of fragments. In such cases any attempt to relate the position of the fragments to the original inserted crack was impossible. There are three interesting features in Fig. 2.

(a) The data for the different tube thicknesses and lengths is unified onto one master curve before any further correction factors are applied. Such scatter that does exist can be found in the data of any individual set.

(b) A linear relationship exists between σ_θ and $(2a)^{-\frac{1}{2}}$ over a limited range of crack length, which does not extrapolate linearly to the origin (i.e $\sigma_\theta = 0$ at $2a = \infty$). Above a particular stress level ($\simeq$ 12 MN m^{-2}) or, alternatively, below a certain crack length ($\simeq$ 3.5 mm), the fracture stress is independent of artificial flaw size.

(c) The transition from single fracture mode of failure to shattering occurs in the middle of the range in which $\sigma_\theta \propto (2a)^{-\frac{1}{2}}$. In an earlier paper [6], it was suggested that the transition in fracture mode might coincide with the change to constant fracture stress which is independent of crack length. Clearly this is not the case. Over the crack length range $0.3 < (2a)^{-\frac{1}{2}} < 0.5$, the length of the inserted crack continues to influence the fracture stress, even though failure results in fragmentation. In this region it is considered that fracture must initiate at the artificial crack tip and then bifurcate to give rise to the fragmentation. Once the crack length is less than 3.5 mm, fracture initiates away from the artificial crack, possibly at the ends of the tube or, alternatively, generally throughout the body.

3.2. Finite width correction

Since the crack length/specimen length ratio reaches 0.75 for the largest cracks, finite width effects will occur, causing the observed fracture stresses to be lower than those required to cause fracture if the cracks were included in infinitely wide plates. For an infinitely wide plate the critical stress intensity factor is given by

$$K_{IC} = \sigma_c(\pi a)^{\frac{1}{2}}. \quad (2)$$

For a plate of finite width, W, the plane strain stress intensity factor is given by [1],

$$K_{IC} = Y\sigma_f a^{\frac{1}{2}} \quad (8)$$

where σ_c and σ_f are the respective uniaxial stresses required for fracture and where $Y = \pi^{\frac{1}{2}} + 0.227\,(2a/W) - 0.51\,(2a/W)^2 + 2.7\,(2a/W)^3$. From Equations 2 and 8 it follows that $\sigma_c/\sigma_f = Y/\pi^{\frac{1}{2}}$. Hence, the effect of including the crack in a plate of finite width, W, is to reduce the average stress required for fracture by the factor $Y/\pi^{\frac{1}{2}}$. Equation 8 was derived for flat plates. Its application in the present case to flawed tubes is due to the absence of the equivalent finite width correction for flawed tubes. As previously stated, the stress system in the present case is predominantly uniaxial and, therefore, very similar to that in the flat plate. Provided the tube diameter is sufficiently large (i.e. the plate curvature slight in the vicinity of the crack), it is considered that the finite width corrections will be similar to those for flat plates.

Fig. 3 shows the fracture data of Fig. 2 increased by the factor $Y/\pi^{\frac{1}{2}}$. σ_{f_1} is then the fracture stress for the equivalent infinite length tube containing the crack of length $2a$. The same general pattern can be seen in both Figs. 2 and 3. The extrapolated line at large crack lengths intersects the abscissa much closer to the origin in Fig. 3 than in Fig. 2, but still does not satisfy the condition $\sigma = 0$ when $2a = \infty$.

Since the expression for Y is a power series in $2a/W$, correction for finite width should be more marked in the case of the shorter specimens. In Fig. 2, the data for the short specimens (25.4 mm long, 0.762 mm thick) generally lie on or below the mean line drawn over the range $0 < (2a)^{-\frac{1}{2}} < 0.5$, while those for the 50.8 mm long, 0.762 mm thick tubes generally lie on or above the line. Correction for finite width causes these two sets of data to become superimposed on a common line (Fig. 3).

The finite width correction applied to the impact data improves the normalization of the data but does not remove all the anomalies.

3.3. Correction for bending effects

The internal pressure is a radial force acting on all parts of the tube. Well away from the crack, this radial force is restrained by the hoop stress. However, the radial forces acting along the edge of the crack bend the edges to give greater radial displacements than at other points of the tube. Bending further increases the local stress at the crack tip for a given nominal hoop stress. Hence

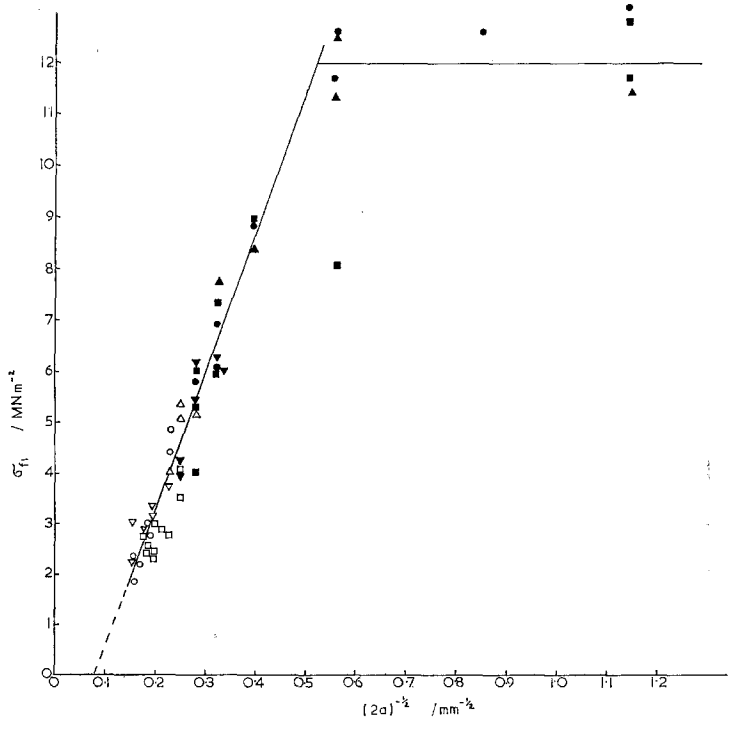

Figure 3 Variation of fracture stress with $(2a)^{-\frac{1}{2}}$ when data presented in Fig. 2 are corrected for finite width effects. (Nomenclature for graphical symbols identical to those given with Fig. 2.)

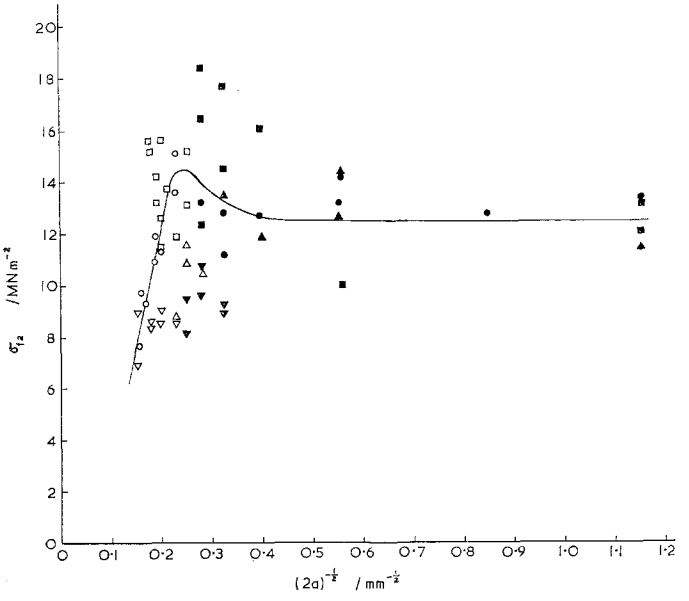

Figure 4 Fracture stress data after application of the bending correction factor to data presented in Fig. 2. (Nomenclature for graphical symbols identical to those given with Fig. 2.)

the fracture stress values shown in Fig. 3, due to the bending effect, will be lower than those required to fracture an infinitely wide flat plate. The stress intensity factor proposed by Folias for an internally pressurized tube containing an axial crack is

$$K_{IC} = \sigma_f (\pi a)^{\frac{1}{2}} \left(1 + 1.67 \frac{a^2}{Rt}\right)^{\frac{1}{2}}. \qquad (5)$$

Comparison of this equation with Equation 2 shows that the mean stress, σ_{f_2}, required to fracture the tube is a factor of $(1 + 1.67a^2/Rt)^{\frac{1}{2}}$ less than that required to fracture an infinitely wide flat plate containing the same crack. Hence increasing the fracture stress data in Fig. 3 by this factor should give the stresses required for fracture of the equivalent flat plate, and the data should then fit Equations 2 and 3 and extrapolate to the origin.

Fig. 4 shows the fracture data given in Fig. 2 (i.e. before finite width correction) corrected for bending effect. Fig. 5 shows the same fracture data corrected for both bending and finite width effects. It can be seen that applying the bending correction scatters the data and increases rather than reduces the anomalous effects. The line drawn in Fig. 4 merely reproduces that given in the previous publication for the 50.8 mm long, 0.762 mm thick set of data, and is not intended to be a best fit to the data. Addition of the data for the other sets of specimens in Fig. 4 shows that no clear trends exist. Application of both

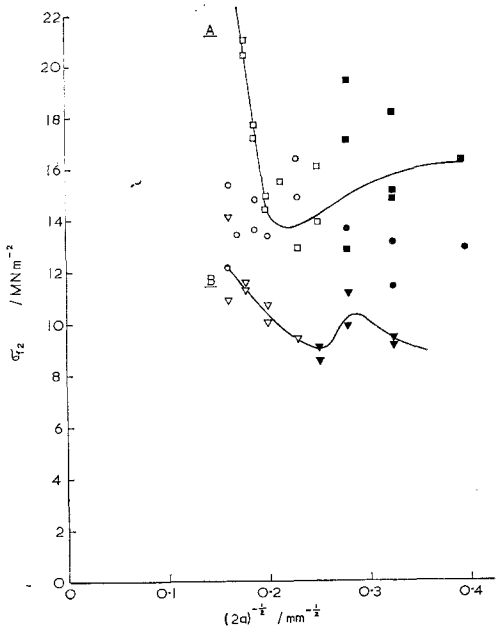

Figure 5 Fracture stress data after application of both finite width and bending correction factors to data presented in Fig. 2. (Nomenclature for graphical symbols identical to those given with Fig. 2.)

finite width and bending correction factors in fact causes a reversal of the general trends as shown in Fig. 5. Curves A and B sketched in Fig. 5 show the manner in which the fracture stresses are predicted to vary with $(2a)^{-\frac{1}{2}}$ in the

equivalent infinite plates of 0.38 and 1.525 mm thickness respectively. In the single fracture mode region, the fracture stresses vary considerably for the two thicknesses of plate and are predicted to *decrease* with decreasing crack size contrary to all fracture theory.

It must be concluded that the bending correction factor used, which was derived from equilibrium considerations, is not applicable under the dynamic conditions in the present tests.

4. Discussion

The internal pressure required to fracture the notched specimens is found to vary with the flaw size, tube thickness and, to a small degree, the tube length. By determining the fracture stress σ_θ, as given by either the thin or thick walled expressions for the hoop stress in a cylinder, the fracture data for all tube geometries studied can be presented on one master curve. It is then found that, over a limited range of crack lengths, the fracture stress obeys a relationship of the form

$$\sigma_\theta = Aa^{-\frac{1}{2}} - B \qquad (9)$$

where A and B are constants. This differs from the usual fracture mechanics equations, firstly in that the relationship only holds over a limited range of crack lengths and secondly by the inclusion of the constant B. Application of the finite width correction factor serves to normalize the data still further, especially the effect of tube length, and reduces the constant B by 40%. Further application of the bending correction factor to the fracture data under impulsive loading renders the data meaningless. It must be concluded that the bending correction factor quoted is not applicable under conditions of rapid loading. This may be due to the short time scale of the fracture event, which does not permit the bending deflections to reach the values predicted from equilibrium considerations. Consequently, the bending correction factor quoted over estimates the corrections to be applied.

The expressions for the hoop stresses (Equations 6 and 7) in an internally pressurized tube and the correction factors for finite width and bending are derived from equilibrium considerations. Furthermore, in applying the correction factors, it has been assumed that the stress intensity factor is constant for the material under consideration. Since the application of the bending correction factor to the dynamic situation has been questioned, the other expressions must also be briefly examined.

Analysis of the deformation of an unnotched thin walled tube subjected to a travelling shock pulse shows that the strain following the application of the pulse follows a damped oscillatory mode, settling to the equilibrium value after a few cycles [10, 11]. The strain during the oscillatory mode can exceed the equilibrium value, as is verified by experiment [11, 12]. It then follows that, during the period of oscillation, the hoop stress can exceed that predicted by equilibrium considerations. Hence the stresses derived from Equations 6 and 7 and shown in Fig. 2, underestimate the maximum hoop stress slightly. This reduction is transferred to all subsequent graphs and is one possible reason for the inability of the data, when $(2a)^{-\frac{1}{2}} < 0.5$, to extrapolate to the origin.

It is known that the stress intensity factor is rate dependent [13], and that the circumferential strain-rate in the shock pressurized tube is finite and linearly related to wall thickness [8, 11]. It is, therefore, questionable whether the K_{IC} values should be held constant as has been done in Section 3 to obtain the fracture stress for the equivalent infinitely wide flat plate. Provided data for equivalent strain rates is considered, then it seems reasonable to equate the K_{IC} values. However, the decrease in circumferential strain-rate with increasing wall thickness suggests that a further correction could be applied to normalize the data for the effects of K_{IC} variation with strain rate. No such correction has been applied due to the absence of information on the effect of strain-rate on K_{IC} for the material tested.

5. Conclusions

It is concluded that a relationship of the form

$$\sigma_\theta = \left(\frac{2E\gamma}{\pi a}\right)^{\frac{1}{2}} - \sigma_\infty$$

fits the fracture data for the flawed tubes under dynamic loading conditions for a limited range of crack lengths ($2a > 3.5$ mm), regardless of whether the fracture mode is by single crack propagation or shattering. The relationship applies when fracture initiates at the inserted flaw. With crack lengths shorter than 3.5 mm, the hoop stresses generated by the larger shock pulses cause fracture initiation at sites other than the inserted crack. Consequently, the fracture

stress is then independent of inserted crack length.

The relationship for σ_θ is obeyed for a range of tube thicknesses and length, where σ_θ is determined by the simple equilibrium equations for the hoop stress. As previously reported [6], the value of the surface energy, γ, is found to be almost identical to that determined from quasi-static testing of the same material. The necessity to include the constant σ_∞ is now considered to arise from the inability of the expressions derived from equilibrium considerations to apply accurately to the dynamic loading situation. This is especially true for the bending correction factor applied.

Acknowledgements

This work has been carried out with the support of the Procurement Executive, Ministry of Defence and the Science Research Council.

References

1. W. BROWN and J. SRAWLEY, ASTM STP 410.
2. J. G. WILLIAMS and P. D. EWING, in "Fracture 1969" (Chapman and Hall, London, 1969).
3. A. A. GRIFFITH, *Phil. Trans. Soc.* **A221** (1921) 163.
4. G. P. MARSHALL and J. G. WILLIAMS, *J. Mater. Sci.* **8** (1973) 138.
5. J. P. BERRY, *J. Polymer Sci.* **50** (1961) 107.
6. P. E. REED and H. V. SQUIRES, *J. Mater. Sci.* **9** (1974) 129.
7. E. S. FOLIAS, *Int. J. Fracture Mech.* **1** (1965) 104.
8. P. E. REED, P. NURSE and E. H. ANDREWS, *J. Mater. Sci.* **9** (1974) 1977.
9. S. TIMOSHENKO, "Strength of Materials" (van Nostrand, New York, 1956).
10. S. TANG, *Proc. Am. Soc. Civ.* **EM5** (1965) 4508.
11. P. E. REED and R. SMITH, to be published.
12. J. L. STOLLERY, Ed., "Shock Tube Research" Paper 60 (Chapman and Hall, London, 1971).
13. J. G. WILLIAMS, *Int. J. Fracture Mech.* **8** (1972) 393.

Received 7 February and accepted 10 March 1975.